particles

Article

Original e^- Capture Cross Sections for Hot Stellar Interior Energies

Panagiota Giannaka [1], Theocharis Kosmas [1,*] and Hiroyasu Ejiri [2]

[1] Theoretical Physics Section, University of Ioannina, GR-45110 Ioannina, Greece
[2] Research Center for Nuclear Physics, Osaka University, Osaka 567-0047, Japan
* Correspondence: hkosmas@uoi.gr; Tel.: +30-2651008489

Abstract: The nuclear electron capture reaction possesses a prominent position among other weak interaction processes occurring in explosive nucleosynthesis, especially at the late stages of evolution of massive stars. In this work, we perform exclusive calculations of absolute e^--capture cross sections using the proton–neutron (pn) quasi-particle random phase approximation. Thus, the results of this study can be used as predictions for experiments operating under the same conditions and in exploring the role of the e^--capture process in the stellar environment at the pre-supernova and supernova phase of a massive star. The main goal of our study is to provide detailed state-by-state calculations of original cross sections for the e^--capture on a set of isotopes around the iron group nuclei (^{28}Si, ^{32}S, ^{48}Ti, ^{56}Fe, ^{66}Zn and ^{90}Zr) that play a significant role in pre-supernova as well as in the core–collapse supernova phase in the energy range $0 \leq E \leq 50$ MeV.

Keywords: semi-leptonic charged-current reactions; nuclear electron capture; supernova dynamics; quasi-particle random phase approximation

Citation: Giannaka, P.; Kosmas, T.; Ejiri, H. Original e^- Capture Cross Sections for Hot Stellar Interior Energies. *Particles* **2022**, *5*, 390–406. https://doi.org/10.3390/particles5030031

Academic Editor: Armen Sedrakian

Received: 5 June 2022
Accepted: 30 August 2022
Published: 12 September 2022

1. Introduction

The electron capture on nuclei is a process that occurs when an electron of energy E_e is entering in the field of an atomic nucleus (A,Z) and is captured by the nucleus as a result of their mutual electro-weak interaction, which, within the standard model, is mediated by the $W^{\pm}$ boson exchange. This reaction is represented by [1,2]

$$(A,Z) + e^- \rightarrow (A,Z-1)^* + \nu_e. \quad (1)$$

Z and A denote the nuclear charge and mass number, respectively, of the initial nucleus. The produced ν_e neutrino carries away energy E_ν while the daughter nucleus absorbs a part of the incoming electron energy equal to the difference $(E_f - E_i)$ between the initial E_i and the final E_f energy of the initial and the final nuclear states, respectively [3–6]. Under laboratory conditions, the e^- of Equation (1) is presumed to be either an orbital electron (bound in the lowest, K, or in a higher, L, M, etc., energy state), a process known as ordinary nuclear electron capture (in this case $E_e \preceq 2.0$ MeV), or a free electron carrying higher energy than that of an orbital electron. For our purposes in the present work, E_e lies in the energy range $E_e \preceq 50$ MeV which covers the electron capture inside the hot and dense stellar interior [7–10].

In modeling the evolution of massive stars (progenitor stars masses 12–20 $M_\odot$) at the final stages of their life, and specifically during core collapse that finally leads to a supernova (SN) explosion (core–collapse SN type II), the electron capture plays a crucial role [1,2,11,12]. The significance of process (1) in SN explosions was discussed long ago by Bethe et al. [1,2], while, in the work by Fuller et al. [11], individual nuclear electron capture rates were derived by employing available experimental data. The incorporation of these rates in SN simulations leads to quite an improved description of the collapse dynamics. For a recent comprehensive discussion of this topic, the reader is referred to the review

works by Langanke et al. in Ref. [7] and references therein. The main conclusion of these predictions that e^--capture on nuclei dominates over those on free protons, motivated further investigations, but, up to the present, the available nuclear electron capture rates are still limited [13] even though extensive stellar e^--capture rate tabulations are available. We mention, for example, the electron capture rates under collapse conditions derived from individual rates for a great number of individual nuclei in Refs. [14–17]. In these works, most of the nuclei which dominate in the early stage of the collapse and nuclei which dominate at high densities are included.

The lack of detailed cross sections predictions throughout the chart of nuclides motivated our present calculation. In Ref. [18], the corresponding stellar electron capture rates are presented evaluated through the well-known folding procedure [3]. On other hand, electron capture rate calculations coming out of shell model diagonalization are available [9,10,19]. In these works, e-capture rates were computed by using various shell model parametrizations for given temperatures of the environments of SNe Ia, while, more recently, an updated table with modern shell-model rates was published by Suzuki et al. [19] (see also Refs. [20,21]). The electron capture in type Ia supernova was discussed previously by Brachwitz et al. [22].

In the early stages of the collapse (type II Supernovae), the e^--capture on nuclei induces a rapid contraction of the massive star's core because it reduces the electron to proton ratio Y_e [2,17,23]. It is now well known that predictions of the reaction rates of the electron capture (also those of its lepton conjugate process of the β-decay) for medium, heavy and very heavy nuclear isotopes, in an environment with high densities and high temperatures relevant to stellar evolution at the final stage, are significant for supernova modeling [6,17,23–29]. Furthermore, electron capture plays an important role in the production of the chemical elements, in particular the heavy elements, through the two major contributors, Supernovae type II and type Ia [30–32]. In a type Ia Supernova, the burning front moving outwards passes along the star triggering the star's explosion [22,33]. In this phase, the electron capture on nuclei occurs in the burning front leading to isotopes with larger neutron excess [19–21] (see also Ref. [22]).

From a nuclear theory viewpoint, up to now for the description of the electron capture process, various microscopic nuclear models have been used as follows: the independent particle model [11], the shell model for s-d shell nuclei [14] and p-f shell model [8], the ordinary random phase approximation (RPA) [15,17], the quasi-particle RPA (QRPA) [3,34], the deformed QRPA [35,36], the continuum RPA (CRPA) [37], the thermal QRPA [38], the large scale shell model [16,30], etc. [39]. Each of these methods has its advantages and disadvantages but many of the calculations, like e.g., [14–16], are comprehensive and tedious. What is, however, worth noting at this point is the fact that the above stellar e-capture results cover a small portion of the input required in many of the SuperNova (SN) explosion codes designed to follow SN explosions and predict the multi-messenger signatures of many important astrophysical phenomena [24,40], while large uncertainties still remain for neutron-rich nuclei and nuclei beyond A = 65, although significant progress has been made in bench marking theoretical electron capture rates [38,41]. Furthermore, rates of e^--capture on nuclei in the region $A \sim 80$ and $N \sim 50$ of the chart of nuclides are required to clarify open questions related to the core–collapse dependence on nuclear electron capture [38,41,42]. We mention that, among other relevant codes [43–45], the known TALYS statistical type code has been recently employed to provide reaction rates towards creating extended database results for nucleosynthesis and stellar evolution studies; see e.g., Ref. [46] and references therein.

In the majority of the above studies, a number of simplifying assumptions (zero momentum transfer to the target nucleus, forward scattering angles, low excitation energies in the final nucleus, schematic nucleon-nucleon interaction, etc.) have been made. Under these assumptions, the authors found that the Gammow–Teller (GT) operator ($\mathrm{GT}^{\pm} = \sum_j \tau_j^{\pm} \sigma(j)$) with $\Delta T = 1$, $\Delta L = 0$, $\Delta J^{\pi} = 1^+$ dominates the electron capture reaction cross sections. The strategy to describe stellar electron capture is derived by

Juodagalvis et al. [47] and is summarized in the recent review by Langanke et al. [7]. In this review, the reader may also find improved shell model studies as e.g., those by Suzuki et al. (see, e.g., [19]. The Gamow–Teller transitions dominate the e^--capture at $E_e \leq 30$ MeV [47,48], an energy region which corresponds to low stellar densities and early core collapse SN, where the studied nuclei have significant abundance in the stellar interior composition. As shown in Ref. [26], in light and medium nuclei, the shell model can describe reliably the GT distributions in nuclei and, hence, the derived stellar electron capture rates for nuclei that are abundant at relatively low stellar densities [19].

Even though these methods are still reliable and the results obtained were interesting, several important details are missing and also some computations need to be further improved. The energies E_e chosen in this work are extended up to $E_e \leq 50$ MeV. In the region, however, $30 \leq E_e \leq 50$ MeV, the abundances of the chosen nuclei must be considered to be smaller or much smaller to those assumed in Ref. [47,48], where authors found that, with increasing E_e, other multipolarities contribute important cross sections, a result which is verified in the present work as we can see in Section 3.

In the present work, detailed e^--capture cross sections are obtained within the framework of a refined version of the quasi-particle RPA (QRPA) [3,34,49]. This method provides the accessible final states of the daughter nuclei in the reaction (1), i.e., all the excited states included in the chosen model space which in the case of QRPA could be relatively rich. It has been employed previously in other charge changing nuclear processes [50–58]. The method is usually tested through the reproducibility of nuclear ground state properties, of various electron scattering data, beta-decay rates and also experimental muon capture rates [34]. The corresponding QRPA predictions may come out of state-by-state calculations of the exclusive, partial and total rate transition matrix elements [59–65]. The agreement with experimental data found in Refs. [3,34] by employing the proton–neutron QRPA (pn-QRPA) with a rich model space and adopting a realistic nucleon–nucleon interaction (the CD-Bonn potential) provided a confidence level and encouraged its use also in electron capture cross section calculations [34]. We mention that this method has been utilized for the evaluation of the nuclear transition matrix elements required to describe the electron capture process in the light nucleus ^{28}Si in Ref. [34].

Our realistic electron capture cross section calculations for the set of isotopes ^{28}Si, ^{32}S, ^{48}Ti, ^{56}Fe, ^{66}Zn and ^{90}Zr may be applicable in supernova dynamics and explosive stellar nucleosynthesis [40,66]. The particular motivation is to explore the role of this reaction in pre-supernova and core–collapse supernova phase. Towards this purpose at first, we assume that this process takes place under laboratory conditions with electrons of energy in the range $0 \leq E_e \leq 50$MeV. Then, because these isotopes play a prominent role in stellar nucleosynthesis [48,67–70], in the next step, we will translate these capture rates, as described in Ref. [18], to those under stellar conditions through the use of a special folding procedure [34].

Since the contribution of the GT operator dominates the total electron capture rates [6,13,17,23,25,33], the quenching effect of the axial-vector coupling g_A that requires special treatment is considered [71–73]. Up to some extent, the g_A value manipulates the differences of the results obtained through the various nuclear methods. In studying this effect, several calculations performed adopted a rather strong quenching ($g_A \sim 0.8$) [6,25,59,71–77]. In the works of Refs. [6,23,25,75], for charge-changing nuclear processes (like the e^--capture), a moderate quenching of g_A has been considered. In our calculations, we also adopt a rather moderate quenching. Of course, for our present results, we avoid the fine-tuning of g_A values since this is time-consuming. We calculate, however, contributions to the total e^--capture cross sections coming out of the entire excitation spectrum of the final nucleus, by considering explicit momentum dependence of the operators.

In the remainder of the paper, at first (Section 2), we describe briefly the nuclear method used for computing absolute e^--capture cross sections within the Donnelly–Walecka formalism. Then (Section 3), we present the results obtained for a set of promising nuclear

isotopes and discuss them in conjunction with other similar results. Finally (Section 4), the main conclusions extracted from this work are summarized.

2. Formalism of Original e^--Capture Cross Sections

The e^--capture on nuclei is a semi-leptonic charge changing process, the theoretical analysis of which requires the description of weak lepton–nucleon interactions as well as the description of the wave functions of the initial and final nuclear states. In this work, the cross sections of this process, as a function of the incident electron energy E_e, are calculated assuming realistic two body interactions (CD-Bonn potential) and following the steps of the pn-QRPA method as described in Refs. [3,34]. It is worth mentioning that the nucleon–nucleon interactions employed (the CD-Bonn potential) are built upon rich physics at the nucleon–nucleon level and are of high-precision since they have been derived within the context of the meson exchange theory and reproduce the p-p, p-n scattering data [78]. In the literature, they are referred to as "realistic" (not schematic) interactions. Furthermore, other nuclear methods use nucleon–nucleon interactions without such features and, thus, testing of the various nuclear models is not always same. Our pn-QRPA method has been checked on the reproducibility of the experimental muon-capture rates (see Ref. [34]).

The state-by-state calculations of the total e^--capture cross section, involving all the transitions between the initial $|i\rangle$ and any final $|f\rangle$ state, starts from the definition of the differential cross section with respect to the solid angles Ω [25]:

$$\frac{d\sigma}{d\Omega} = \frac{VE_\nu^2}{(2\pi)^2} \sum_{leptons\ spins} \frac{1}{2J_i+1} \sum_{M_i} \sum_{M_f} |\langle f|\widehat{H}_w|i\rangle|^2 \tag{2}$$

(V denotes the normalization volume), where E_ν the energy of the outgoing neutrino. The weak interaction Hamiltonian $\widehat{H}_w$ has the same form as in the case of muon capture process (for more details, see [34]).

In the set of isotopes chosen, the original cross sections for the electron capture process are obtained by the expression (Donnelly–Walecka multipole decomposition method) [79,80].

$$\begin{aligned}
\frac{d\sigma_{ec}}{d\Omega} &= \frac{G_F^2 \cos^2\theta_c}{2\pi} \frac{F(Z,E_e)}{(2J_i+1)} \Bigg\{ \sum_{J\geq 1} \mathcal{W}(E_\nu) \Big\{ [(1-(\hat{\nu}\cdot\hat{\mathbf{q}})(\beta\cdot\hat{\mathbf{q}}))] \left[|\langle J_f\|\widehat{\mathcal{T}}_J^{mag}\|J_i\rangle|^2 + |\langle J_f\|\widehat{\mathcal{T}}_J^{el}\|J_i\rangle|^2 \right] \\
&- 2\,\hat{\mathbf{q}}\cdot(\hat{\nu}-\beta) Re\langle J_f\|\widehat{\mathcal{T}}_J^{mag}\|J_i\rangle\langle J_f\|\widehat{\mathcal{T}}_J^{el}\|J_i\rangle^* \Big\} + \sum_{J\geq 0} \mathcal{W}(E_\nu) \Big\{ (1+\hat{\nu}\cdot\hat{\beta}) |\langle J_f\|\widehat{\mathcal{M}}_J\|J_i\rangle|^2 \\
&+ (1-\hat{\nu}\cdot\beta+2(\beta\cdot\hat{\mathbf{q}}) |\langle J_f\|\widehat{\mathcal{L}}_J\|J_i\rangle|^2 - 2\,\hat{\mathbf{q}}\cdot(\hat{\nu}+\beta) Re\langle J_f\|\widehat{\mathcal{L}}_J\|J_i\rangle\langle J_f\|\widehat{\mathcal{M}}_J\|J_i\rangle^* \Big\} \Bigg\}
\end{aligned} \tag{3}$$

where $\mathcal{W}(E_\nu) = E_\nu^2/(1+E_\nu/M_T)$, with M_T being the mass of the target nucleus, taking into consideration the nuclear recoil, and $F(Z,E_e)$ denotes the well-known Fermi function [68]. The nuclear matrix elements between the initial state $|J_i\rangle$ and a final state $|J_f\rangle$ refer to the Coulomb $\widehat{\mathcal{M}}_{JM}$, longitudinal $\widehat{\mathcal{L}}_{JM}$, transverse electric $\widehat{\mathcal{T}}_{JM}^{el}$ and transverse magnetic $\widehat{\mathcal{T}}_{JM}^{mag}$ multipole operators (see Ref. [34]). In addition, $\hat{\mathbf{q}}$, $\hat{\nu}$ are the unit vectors of the momentum transfer $\mathbf{q}$, the neutrino momentum and $\beta = k/E_e$ with k the corresponding electron 3-momentum.

Within the J-projected multipole decomposition formalism of Donnelly–Walecka, the differential cross section in electron capture on nuclei takes the form

$$\frac{d\sigma_{ec}}{d\Omega} = \frac{G_F^2 \cos^2\theta_c}{2\pi} \frac{F(Z,E_e)}{(2J_i+1)} \cdot \Big\{ \sum_{J\geq 1} \mathcal{W}(E_\nu) \{ [1-\alpha\cos\Phi + b\sin^2\Phi] [|\langle J_f \| \widehat{\mathcal{T}}_J^{mag} \| J_i \rangle|^2 + |\langle J_f \| \widehat{\mathcal{T}}_J^{el} \| J_i \rangle|^2]$$
$$- [\frac{(\varepsilon_i+\varepsilon_f)}{q}(1-\alpha\cos\Phi) - d] 2Re \langle J_f \| \widehat{\mathcal{T}}_J^{mag} \| J_i \rangle \langle J_f \| \widehat{\mathcal{T}}_J^{el} \| J_i \rangle^* \} + \sum_{J\geq 0} \mathcal{W}(E_\nu) \{ (1+\alpha\cos\Phi) |\langle J_f \| \widehat{\mathcal{M}}_J \| J_i \rangle|^2 \quad (4)$$
$$+ (1+\alpha\cos\Phi - 2b\sin^2\Phi) |\langle J_f \| \widehat{\mathcal{L}}_J \| J_i \rangle|^2 - [\frac{\omega}{q}(1+\alpha\cos\Phi) + d] 2Re \langle J_f \| \widehat{\mathcal{L}}_J \| J_i \rangle \langle J_f \| \widehat{\mathcal{M}}_J \| J_i \rangle^* \} \Big\}$$

The kinematical parameters α, b, d are given in Appendix A (see Ref. [50] for more details). In Equation (4), Φ represents the scattering angle while $\omega = E_f - E_i$ denotes the excitation energy of the final nucleus (for forward scattering used by many authors $\Phi = 0$).

The energy, E_ν, of the outgoing neutrino in reaction (1), due to energy conservation, is written as

$$E_\nu = E_e - Q + E_i - E_f \,, \quad (5)$$

where Q is the known Q-value determined from the experimental masses of the parent (M_i) and the daughter (M_f) nuclei as $Q = M_f - M_i$ [25].

At this point, we must mention that, in many works, the exclusive e^--capture cross section from an initial $|J_i\rangle$ to a final $|J_f\rangle$ state was approximated by [25]

$$\sigma_{fi}(E_e) = \frac{6(E_e - E)^2 G_F^2 \cos^2\theta_c}{\pi(2J_i+1)} |\langle J_f \| \widehat{\mathcal{L}}_1 \| J_i \rangle|^2 \quad (6)$$

where the operator $\widehat{\mathcal{L}}_{1M}$ is written as

$$\widehat{\mathcal{L}}_{1M} = \frac{i}{\sqrt{12\pi}} G_A \sum_{i=1}^{A} \tau_+(i) \sigma_{1M}(i) \quad (7)$$

The above expression of the exclusive e^--capture cross section results in the approximation $q \to 0$ (low momwntum transfer). Under these conditions, the transitions of Gamow–Teller operator ($GT_+ = \sum_i \tau_i^+ \sigma_i$) provide the dominant contribution to the total cross section [25].

In this work, we perform detailed calculations for original e^--capture cross sections taking into account not only the contribution of the Gamow–Teller type operator (using quenched value of g_A) but the contributions of all low-spin multipolarities ($J^\pi \leq 5^\pm$). In performing detailed state-by-state calculations for the set of chosen isotopes, we assumed that (i) the initial state of the parent nucleus is a ground state $|0^+\rangle$, and (ii) the nuclear system is under laboratory conditions.

3. Results and Discussion

Our exclusive electron capture cross sections refer to a set of isotopes that cover the light- and medium-weight region of the periodic table. This set includes the light nuclei ^{28}Si and ^{32}S, the medium weight isotopes ^{48}Ti, ^{56}Fe and ^{66}Zn that belong to the iron group nuclei and the heavier ^{90}Zr isotope. The initial $|J_i\rangle$ and the final $|J_f\rangle$ states in Equation (4) are determined by solving the BCS equations, for the ground state [3,34,49,50,81–85] and the pn-QRPA equations, for the excited states [3,34,49,50,53,54], respectively. For the detailed evaluation of the required nuclear matrix elements between the ground and excited states as well as for all other nuclear parameters required for the realistic two body interactions of CD-Bonn potential for the studied isotopes, the reader is referred to Refs. [3,34].

In the calculations of the axial vector contributions to the cross sections presented below, we used the quenched value of $g_A = 1.0$. This value of g_A takes into account a rather small quenching effect indicated for medium-weight nuclei. The value of g_A is introduced through the axial vector form factor $F_A(q^2)$ of the multipole operators, producing all

the possible transitions $0^-, 1^+$, etc. [3,34,64,76,77]. The use of this quenched value of g_A is equivalent to the normalization of the matrix elements of Ref. [25] and predicts experimental results under laboratory conditions. Actually, the g_A for $1^+, 2^-$ derived from beta decays, muon captures and charge exchange reactions suggest much severe quenching factors than that employed here [71–74], but this is going to be further explored elsewhere.

The results presented in this work have been obtained as follows. First of all, we performed realistic detailed state-by-state calculations for exclusive e^--capture cross sections in the above-mentioned set of nuclear isotopes. Then, we focused on a specific incident electron energy (25 MeV) and found the partial contribution of each multipolarity as well as the percentage of their contribution to the total e^--capture cross sections. In the last step of our study, we calculated total e^--capture cross sections and also estimated the individual contributions into the total cross sections of the polar-vector and axial-vector operators.

3.1. State-by-State e^--Capture Cross Sections

In the first step, we performed state-by-state calculations on the electron capture differential cross sections with respect to the excitation energy $d\sigma/d\omega$ defined by

$$\begin{aligned}\frac{d\sigma}{d\omega} \equiv \Big[\frac{d\sigma}{d\omega}\Big]_{excl} &= \frac{G_F^2\cos^2\theta_c}{2\pi}\frac{F(Z,E_e)}{(2J_i+1)}\cdot\Big\{\int d\Omega \mathcal{W}(E_\nu)\,\{[1-\alpha\cos\Phi+b\sin^2\Phi]\,[|\langle J_f\|\widehat{\mathcal{T}}_J^{mag}\|J_i\rangle|^2+|\langle J_f\|\widehat{\mathcal{T}}_J^{el}\|J_i\rangle|^2]\\ &- \Big[\frac{(\varepsilon_i+\varepsilon_f)}{q}(1-\alpha\cos\Phi)-d\Big]2Re\langle J_f\|\widehat{\mathcal{T}}_J^{mag}\|J_i\rangle\langle J_f\|\widehat{\mathcal{T}}_J^{el}\|J_i\rangle^*(1+\alpha\cos\Phi)|\langle J_f\|\widehat{\mathcal{M}}_J\|J_i\rangle|^2 \qquad (8)\\ &+ (1+\alpha\cos\Phi-2b\sin^2\Phi)|\langle J_f\|\widehat{\mathcal{L}}_J\|J_i\rangle|^2-\Big[\frac{\omega}{q}(1+\alpha\cos\Phi)+d\Big]2Re\langle J_f\|\widehat{\mathcal{L}}_J\|J_i\rangle\langle J_f\|\widehat{\mathcal{M}}_J\|J_i\rangle^*\}\Big\}\end{aligned}$$

We started by evaluating the exclusive e^--capture cross sections of Equation (8) for all multipolarities with $J^\pi \leq 5^\pm$ considering incident electron energy equal to $E_e = 25.0$ MeV. In Equation (8), the transition matrix elements are considered to be between the ground state $|J_i\rangle = |i\rangle \equiv |0^+_{g.s.}\rangle$ of a spherical target nucleus and an excited state $|J^\pi_f\rangle \equiv |f\rangle$ of the resulting odd-odd nucleus. The cross sections as functions of the incident electron energy E_e are evaluated after integrating numerically Equation (4) over angles for each specific final state $|J^\pi_f\rangle$.

The excitations of the daughter nucleus in our code appear as sets of multipole states and give us the possibility to calculate the contribution to the total cross sections of each multipole set of states separately. The dependence of the differential cross sections on the excitation energy ω through the entire pn-QRPA spectrum of the daughter nucleus may, afterwards, be illustrated by using a special code which rearranges all possible excitations (with the corresponding cross sections) in ascending order with respect to the energy ω. In the model space chosen for each isotope, for all multipolarities up to $J^\pi = 5^\pm$, we have totally a number of 286 states for ^{28}Si isotope, 440 states for each of the ^{32}S and ^{48}Ti isotopes, 488 states separately for ^{56}Fe and ^{66}Zn isotopes, and 912 states for the ^{90}Zr isotope. The variation of the exclusive rates in the entire excitation spectrum of the daughter nuclei (^{28}Al, ^{32}P, ^{48}Sc, ^{56}Mn, ^{66}Cu, ^{90}Y) is demonstrated in Figures 1–3.

As shown in these figures, the differential electron capture cross sections present some characteristic clearly pronounced peaks at various QRPA excitation energies ω. Under the assumptions of our present work, these peaks correspond mainly to $1^\pm$ and $0^\pm$ transitions. In further detail, starting from the lightest daughter nucleus, ^{28}Al presents two characteristic peaks i.e., the first at $\omega = 0.968$ MeV corresponding to the 0^+_1 transition and the second at $\omega = 7.712$ MeV corresponding to the 1^+_7 transition. The ^{32}P nucleus has only one clearly pronounced peak at $\omega = 4.855$ MeV corresponding to the 1^+_7 transition. The ^{48}Sc nucleus presents one peak at $\omega = 3.575$ MeV for the 1^+_2 transition and another one at $\omega = 4.319$ MeV for 0^+_1 transition. In the case of ^{56}Mn, the characteristic peaks appear at $\omega = 0.163$ MeV and $\omega = 2.412$ MeV and correspond to the 1^+_1 and 0^+_1 transitions, respectively. The other two peaks, corresponding to 0^+_1 and 1^+_{10} transitions, appear at $\omega = 2.538$ MeV and $\omega = 6.555$ MeV, respectively, for the ^{66}Cu daughter nucleus. Finally,

the isotope ^{90}Y presents the maximum peak at $\omega = 4.376$ MeV for the 0^+_2 transition, a peak at $\omega = 1.818$ MeV for the 1^+_1 transition and for the 1^+_{16} transition a characteristic peak at $\omega = 8.643$ MeV.

Focusing on the extensively studied previously ^{56}Fe isotope, we compare our results with existing experimental data of ^{56}Fe(d,^{2}He)^{56}Mn and ^{56}Fe(n,p)^{56}Mn reactions. The ^{56}Fe(d,^{2}He)^{56}Mn experiment [86] set clearly two strong transitions to 1^+ states at 0.11 MeV and 1.2 MeV, which are in rather good agreement with our results as we find the first at 0.163 MeV and the second at 0.881 MeV. In addition, the ^{56}Fe(n, p) experiment [87] set three characteristic peaks in the energy range 0–2 MeV (the first two peaks are in very good agreement with our peaks). In addition to the agreement of our results with the experimental data, they are also compared well with the findings coming from the theoretical studies of the e^--capture process using different theoretical approaches.

In Refs. [6,88], using the QRPA method with a different two-body interaction, Nabi et al. set the first peak at about 0.2 MeV. Furthermore, Langanke et al. [30] in their predictions using a large-scale shell model found a peak near 0.1 MeV with their clearly pronounced peak to be placed at about 1.7 MeV. Similar conclusions are extracted for the ^{48}Ti isotope where the data from the ^{48}Ti(n, p) experiment [89] peaks at about 3 MeV, a 1^+ multipole, and, from the ^{48}Ti$(d,^2$He) experiment [90], the major peak appears at about 3.2 MeV.

With our method, we found the major peak for 1^+ transitions at about 3.5 MeV, in good agreement with experimental data. Other theoretical approaches, using the QRPA method [23], placed the major peak of 1^+ multipolarity of the ^{48}Ti daughter nucleus at about 3 MeV also in good agreement with our results. The comparison of the peaks shown from our state-by state e^--capture calculations with the experimental data and the other theoretical predictions provides us with a high confidence level regarding the method utilized.

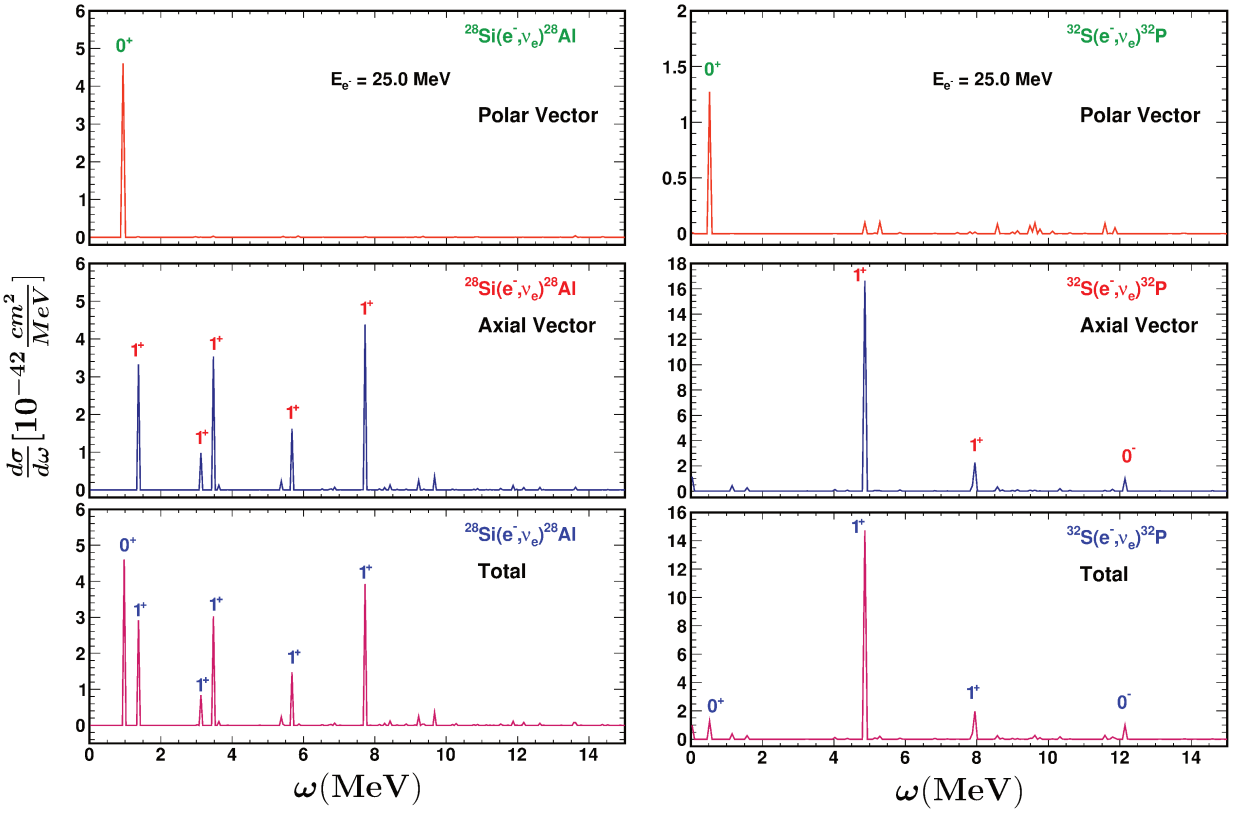

Figure 1. Total differential electron capture cross sections, $d\sigma/d\omega$, as a function of the excitation energy ω and individual contribution of the Polar-Vector, Λ_V, and Axial-Vector, Λ_A, operatorss, for the ^{28}Si and ^{32}S nuclei.

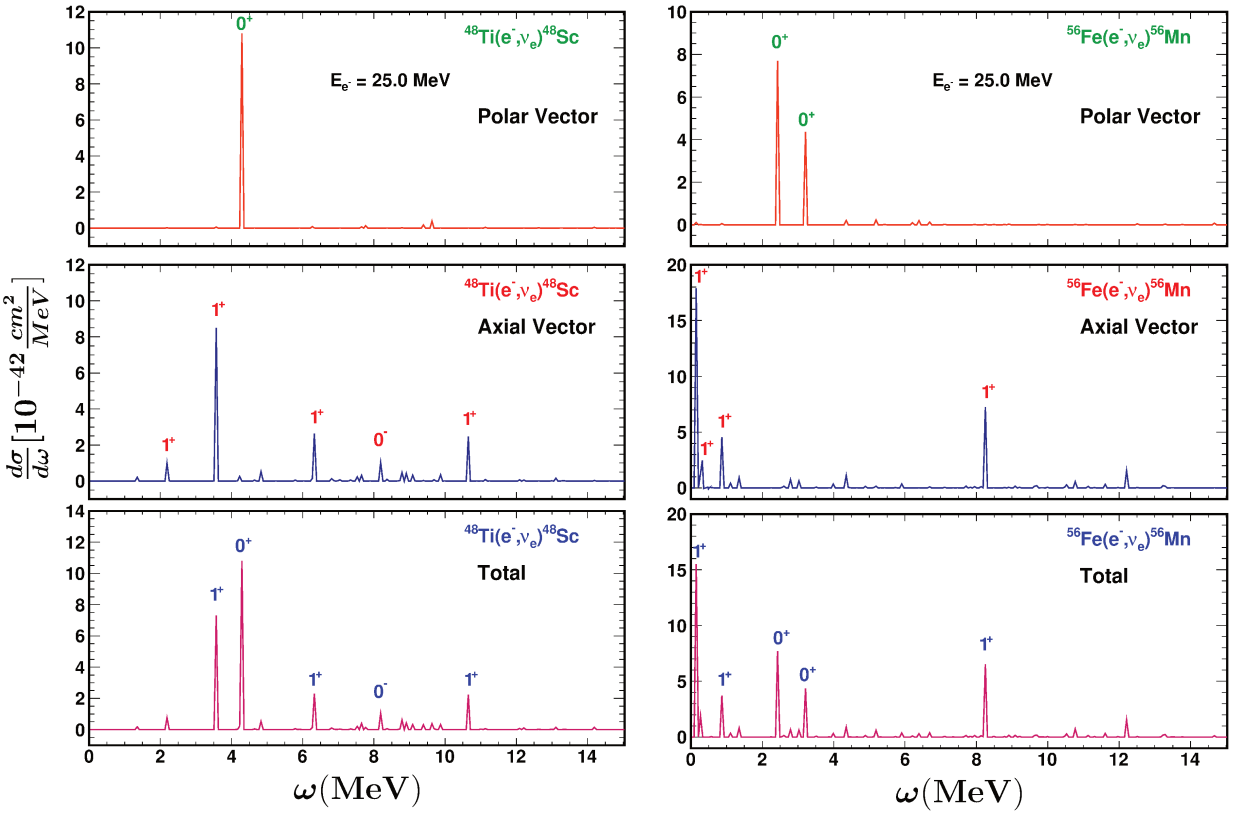

Figure 2. The same as Figure 1 but for the ^{48}Ti and ^{56}Fe nuclei.

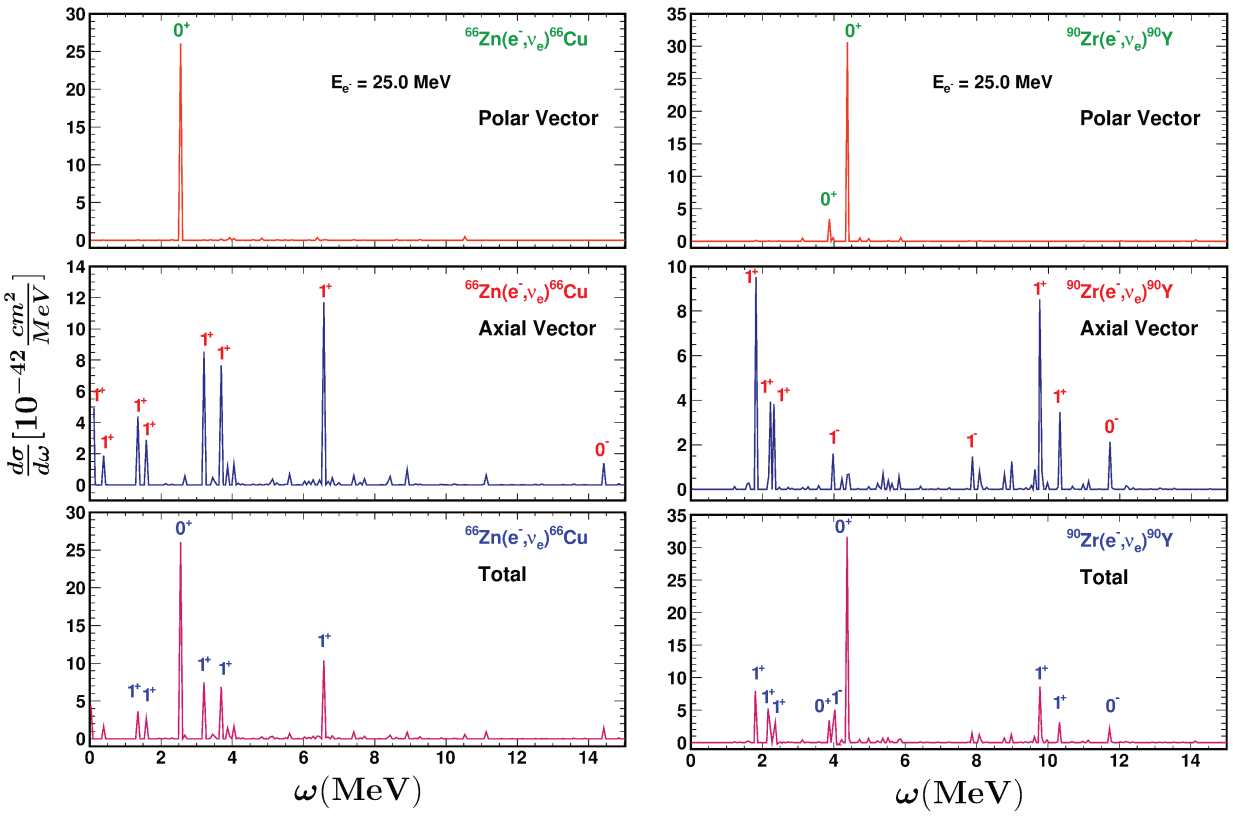

Figure 3. The same as Figure 1 but for the ^{48}Ti and ^{56}Fe nuclei.

From the illustration of the state-by-state calculations of the absolute e^--capture cross sections in Figures 1–3, it becomes obvious that the main contribution comes from the 1^+ multipolarity. As our code has the possibility to provide the contribution of polar-vector and axial-vector terms separately for each multipolarity, we can see in detail which peaks in the above figures come from each term. As expected, the axial vector terms provide mainly the contribution of 1^+ multipolarity (the polar vector terms contribute the 0^+ multipolarity).

Closing this subsection, we note that all figures of this subsection have been designed by using the ROOT program of CERN with binning width 0.05 for ^{28}Si and ^{90}Zr isotopes, 0.06 for ^{48}Ti, ^{56}Fe and ^{66}Zn isotopes, and 0.07 for ^{32}S.

3.2. Individual Contribution of Each Multipolarity

The second stage of our study includes calculations of the partial e^--capture cross sections coming out of the low-spin multipolarities (for $J^\pi \leq 5^\pm$). These partial e^--capture cross sections result by summing over the contributions of all the individual multipole states of a given multipolarity as

$$\sigma_{J^\pi} \equiv \left[\frac{d\sigma}{d\omega}\right]_{part} = \sum_f \left[\frac{d\sigma}{d\omega}\right]_{excl} \tag{9}$$

The results obtained from the partial e^--capture cross sections for the chosen nuclei are illustrated in Figure 4. It is obvious that, for all isotopes, the main contribution to the total e^--capture cross section (for $E_e = 25.0$ MeV) comes from the 1^+ transitions (some 0^+ transitions contribute notable portion to the total rate). From the rest of the multipolarities, the 0^-, 1^- and 2^- transitions are less important while other multipolarities offer rather negligible contributions.

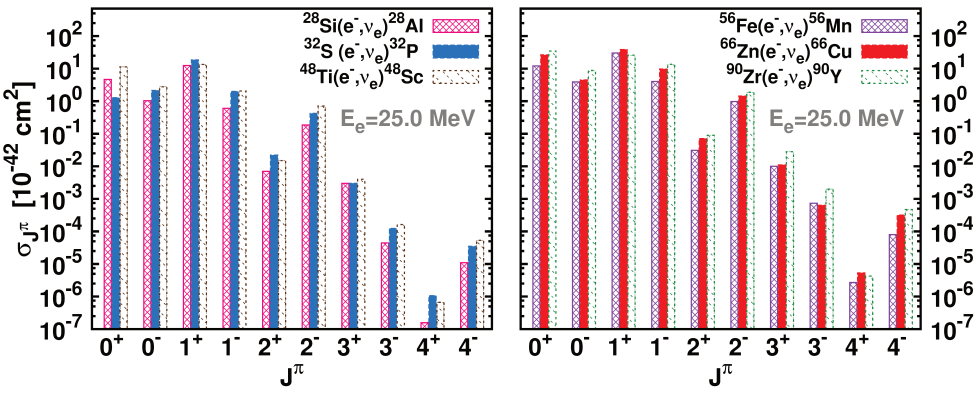

Figure 4. Partial e^--capture cross sections originating from different multipole transitions for all isotopes.

In Table 1, the exact contributions of the low-spin individual multipolarities J^π are listed, while, in Table 2, the portions of each multipolarity into the total rate are shown. Obviously, in the energy range of our present calculations, only for the light nuclei ^{28}Si and ^{32}S can the contribution of the 1^+ multipolarity be considered dominant. In such a case, the main portion of the total e^--capture cross sections may be considered that comes from the Gamow–Teller type operator. For medium-weight and heavy nuclei, contributions coming from other multipolarities (especially the 0^+, 1^-, etc.) are significant and can not be omitted.

Specifically, as the mass number of the nucleus increases, the contribution of other multipolarities also increases and the contribution of 1^+ multipolarity decreases. Moving towards higher incident electron energies, the contribution of the other multipolarities becomes comparable with that of 1^+ (see also below). For example, at $E_e = 40.0$ MeV, for the ^{56}Fe isotope, the contribution of all 0^+ is about 18% and that of all 1^+ 38%. For ^{66}Zn, the corresponding contributions are about 24% and 31%, while, for ^{90}Zr, they are

about 28% and 20%, respectively. These results show the significance of including all the multipolarities into the calculations of total e^--capture cross sections in high incident e^--energies and in heavy isotopes.

Table 1. Individual contribution σ_e (in 10^{-42} cm^2) of low-spin multipolarities (up to $J^\pi = 5^\pm$) to the total electron capture cross sections (at E_e = 25 MeV), evaluated with the pn-QRPA method.

	^{28}Si	^{32}S	^{48}Ti	^{56}Fe	^{66}Zn	^{90}Zr
0^+	4.657	1.275	11.361	12.062	26.450	34.561
0^-	1.036	2.131	2.784	3.916	4.466	8.739
1^+	12.534	18.529	13.477	30.299	38.426	25.863
1^-	0.606	2.007	2.052	4.018	9.726	13.696
2^+	0.007	0.022	0.015	0.031	0.071	0.089
2^-	0.185	0.421	0.709	0.980	1.438	1.875
3^+	0.003	0.003	0.004	0.010	0.011	0.028
3^-	0.445×10^{-4}	0.124×10^{-3}	0.164×10^{-3}	0.735×10^{-3}	0.637×10^{-3}	0.201×10^{-2}
4^+	0.157×10^{-6}	0.106×10^{-5}	0.668×10^{-6}	0.270×10^{-5}	0.534×10^{-5}	0.426×10^{-5}
4^-	0.110×10^{-4}	0.346×10^{-4}	0.532×10^{-4}	0.799×10^{-4}	0.316×10^{-3}	0.471×10^{-3}
5^+	0.753×10^{-8}	0.785×10^{-7}	0.537×10^{-6}	0.888×10^{-6}	0.397×10^{-6}	0.832×10^{-5}
5^-	0.483×10^{-9}	0.289×10^{-9}	0.238×10^{-8}	0.600×10^{-8}	0.291×10^{-7}	0.541×10^{-7}

Table 2. The percentages of low-spin multipolarities (up to $J^\pi \leq 3^\pm$) into the total e^--capture cross sections, evaluated with our pn-QRPA method.

	^{28}Si	^{32}S	^{48}Ti	^{56}Fe	^{66}Zn	^{90}Zr
0^-	5.45	8.74	9.16	7.63	5.54	10.30
0^+	24.47	5.23	37.37	23.51	32.82	40.73
1^-	3.19	8.23	6.75	7.83	12.07	16.14
1^+	65.86	75.97	44.33	59.04	47.68	30.48
2^-	0.98	1.73	2.33	1.91	1.78	2.21
2^+	0.04	0.09	0.05	0.06	0.09	0.10
3^-	∼0.00	∼0.00	∼0.00	∼0.00	∼0.00	∼0.00
3^+	0.01	0.01	0.01	0.02	0.01	0.03

It should be noted that, for the ^{48}Ti, ^{56}Fe, ^{66}Zn and ^{90}Zr isotopes having $Z < N$, our pn-QRPA gives a bit higher 0^+ and 1^- contributions to the total e^--capture cross sections as compared to some other methods. This holds also for some other charge-changing processes like the inelastic neutrino-nucleus scattering, muon capture, etc. We mention, however, that similar recent theoretical estimations of 0^+ contributions in single charge exchange reactions using another type of pn-QRPA are much smaller than the corresponding experimental data (see, e.g., Table V in Ref. [91]), which implies that our method gives results towards the correct direction.

3.3. Original Total Electron Capture Cross Sections

In the next stage of the present study, we computed original total cross sections σ_e for e^--capture on the chosen set of nuclei. They result by summing over all the individual

contributions of the final states. At first, we performed it for the states of each specific multipolarity, and then we summed over the low-spin multipolarities (up to $J^\pi = 5^\pm$) as

$$\sigma_e \equiv \sum_{J^\pi} \left[\frac{d\sigma}{d\omega}\right]_{part} = \sum_{J^\pi}\sum_{f} \left[\frac{d\sigma}{d\omega}\right]_{excl} \tag{10}$$

For these calculations, we use the expression of Equation (4). As mentioned before, in performing these calculations, we assumed that the initial state of each parent nucleus is the $|0^+\rangle$ ground state.

The obtained total electron capture cross sections for all studied target nuclei are illustrated in Figures 5–7 where the individual contributions of the various channels ($J^\pi \leq 5^\pm$) are shown. These Figures, for very low electron energies, E_e equalling up to a few MeV above threshold, exhibit a sharp increase of the electron capture cross sections by several orders of magnitude. This reflects the variation with the incident energy E_e of the GT^+ strength distribution. In even-even parent nuclei, the GT^+ strength, is centred at daughter excitation energies of the order of 2 MeV. Thus, the e^--capture cross sections for these nuclei increase drastically within the first couple of MeV. For electron energy $E_e \geq 10$ MeV, the calculated cross sections show a moderate increase. Obviously, for triggering the e^--capture process, a minimum electron energy, given by the mass difference between parent and daughter nuclei ($M_f - M_i =$ Q-value of the process), is required.

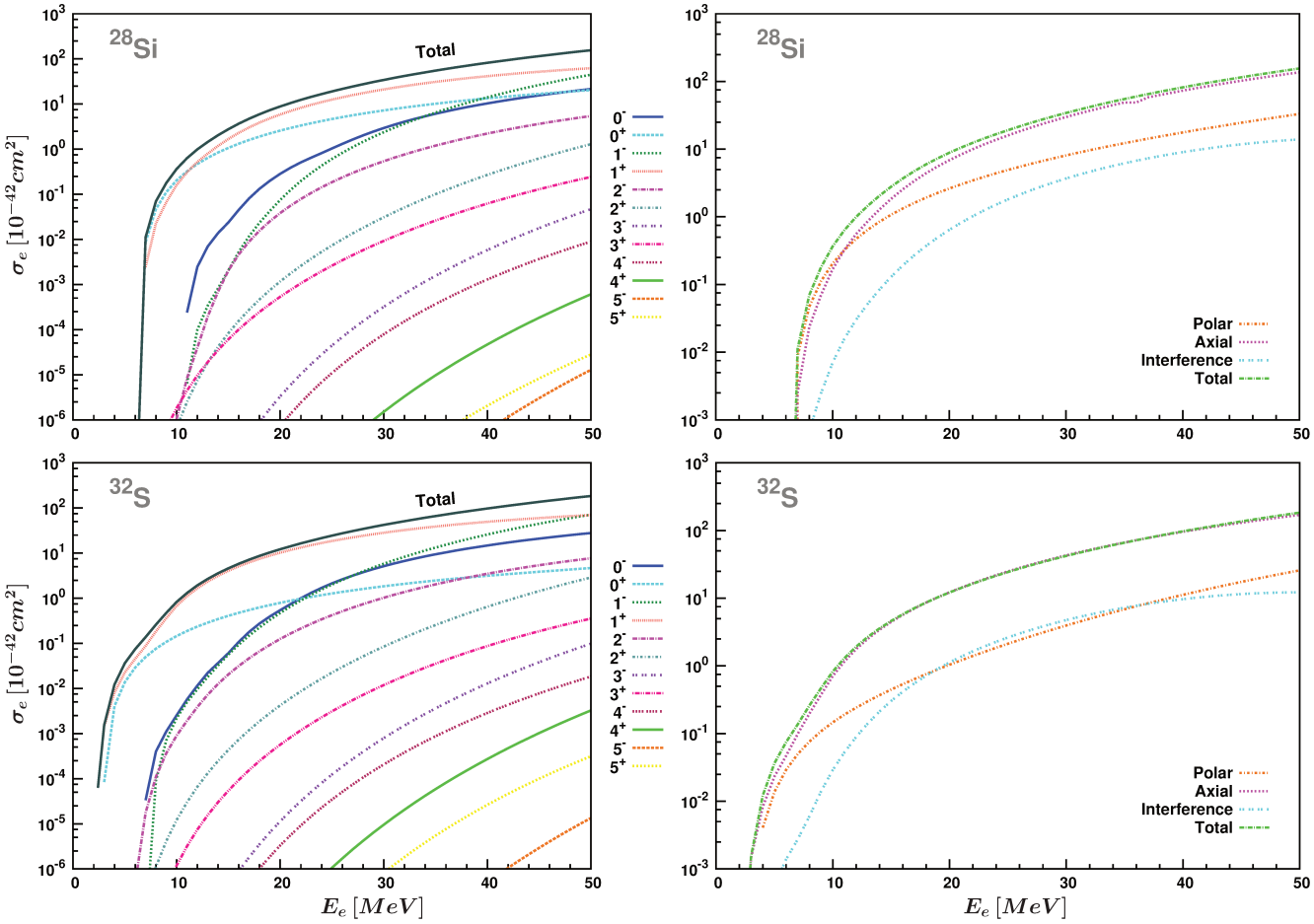

Figure 5. The individual contribution to the total e^--capture cross sections (bold, full line) of various channels ($J^\pi \leq 5^\pm$) are demonstrated in this figure in ^{28}Si$(e^-, \nu_e)^{28}$Al and ^{32}S$(e^-, \nu_e)^{32}$P reactions. Moreover, in the right part of each figure, the individual contribution of the polar-vector, axial-vector and interference terms are also illustrated.

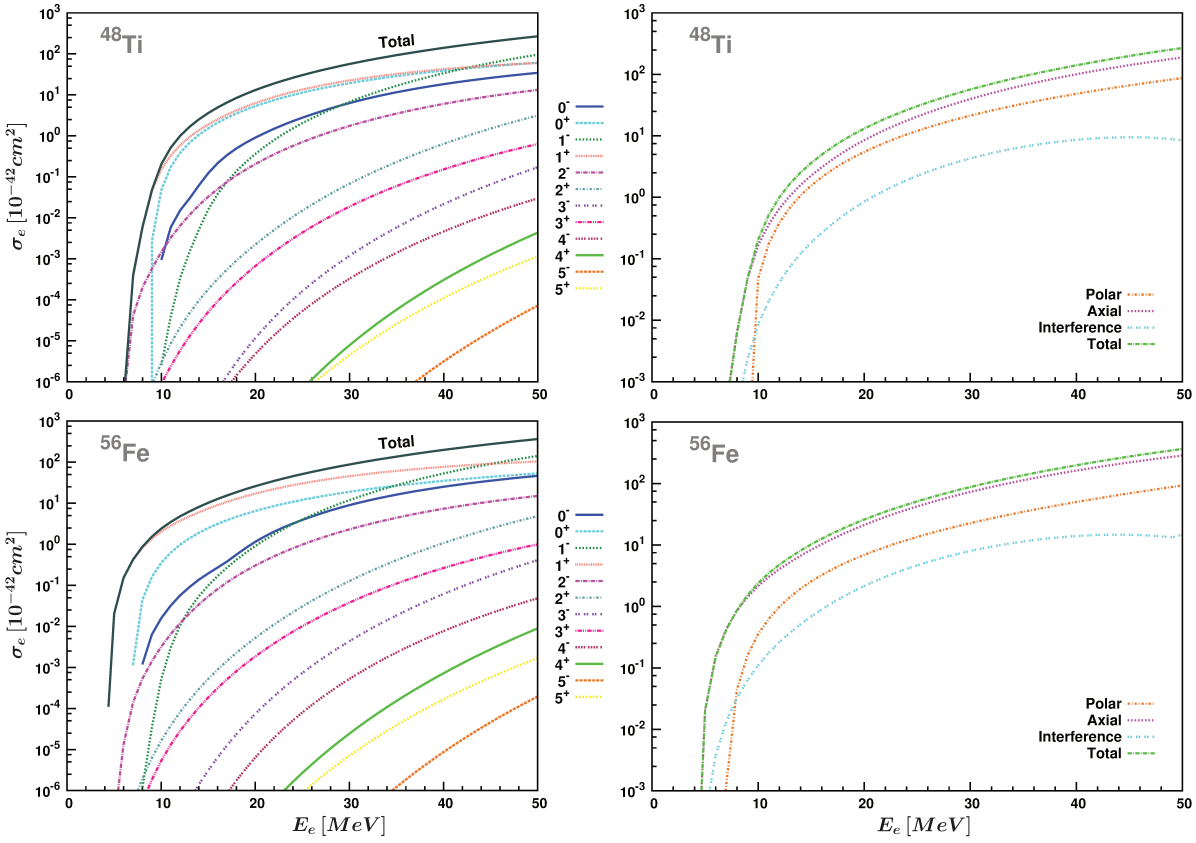

Figure 6. The same as Figure 5 but for $^{48}\mathrm{Ti}(e^-,\nu_e)^{48}\mathrm{Sc}$ and $^{56}\mathrm{Fe}(e^-,\nu_e)^{56}\mathrm{Mn}$ reactions.

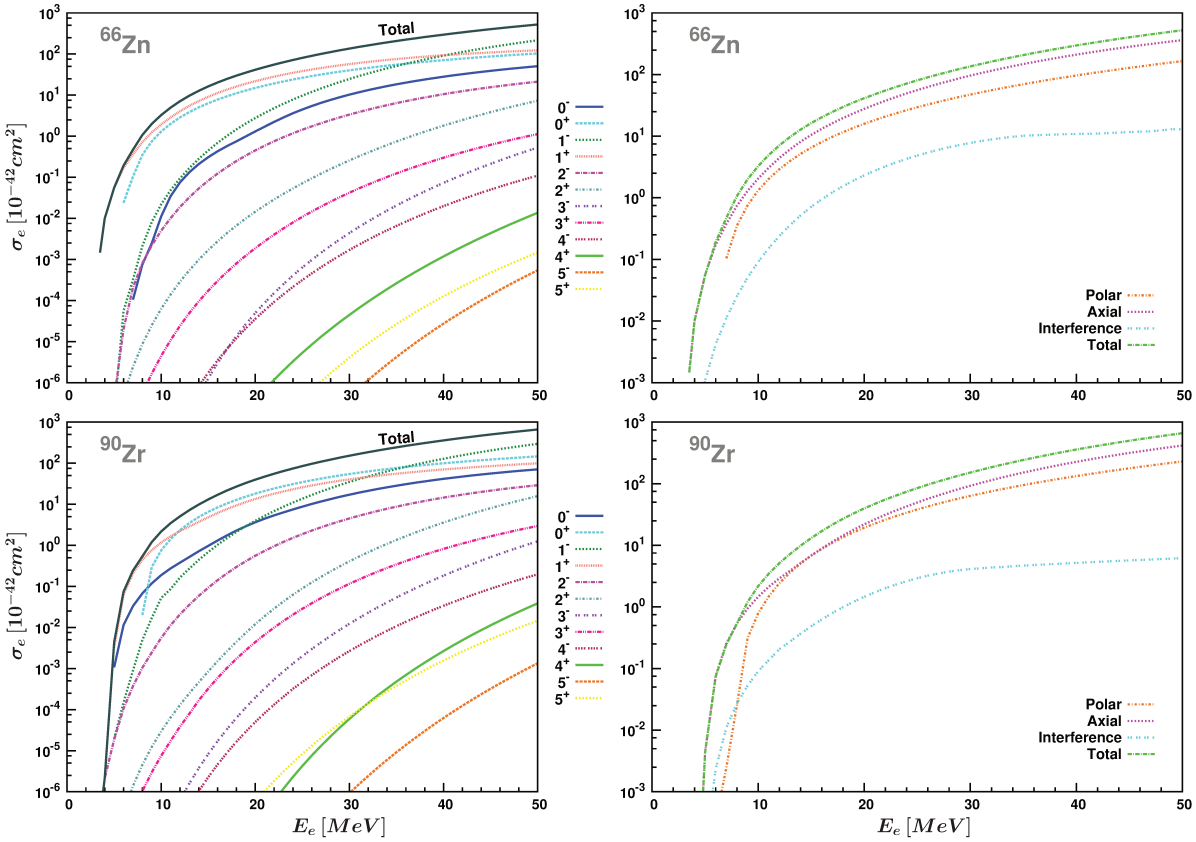

Figure 7. The same as Figure 5 but for $^{66}\mathrm{Zn}(e^-,\nu_e)^{66}\mathrm{Cu}$ and $^{90}\mathrm{Zr}(e^-,\nu_e)^{90}\mathrm{Y}$ reactions.

3.4. Impact to Experiments Nuclear Physics and Astrophysics

From an experimental and astrophysics point of view, the important energy range of the incident electron, E_e, in the e^--capture process raises up to 30 MeV [9,10]. In this region, we observe that the 1^+ multipolarity has the largest contribution to the total electron capture cross sections [25]. Specifically, starting from the light parent nuclei of our chosen set, ^{28}Si and ^{32}S, the portions of the contribution of the 1^+ multipolarity in this region are larger than 60%. For the medium weight parent nuclei ^{48}Ti, ^{56}Fe and ^{66}Zn, the corresponding portions in this region are larger than 40%. Due to this effect, many authors focused on this energy region and calculated only the contribution of the 1^+ multipolarity to the total electron capture cross sections. However, using our method, for the medium-heavy parent nucleus ^{90}Zr, we find that the contribution of 1^+ multipolarity to the total e^- is just about 25%. Obviously, in systematic calculations of electron capture rates on heavier and more neutron rich nuclei, contributions coming from forbidden transitions should also be included in addition to the GT^+ channel [9,10,36,86]. For this reason, more accurate calculations of the total e^--capture cross sections are obtained by taking into account the contributions of all possible multipolarities at least up to $J^\pi = 5^\pm$.

In the present work, we have chosen as highest incident electron energies E_e up to 50 MeV, since, at higher energies, the contribution of other multipolarities like 1^-, 0^+ and 0^- of the chosen set become noticeable and can not be omitted. As can be seen from Figures 5–7, for all studied light and medium weight nuclei, at energies around 40 MeV, the contribution of the 1^- multipolarity becomes significant and overcomes even the contribution of 1^+ multipolarity. For the heavy nucleus ^{90}Zr, in contrast to the other nuclei, the contribution of all 1^- states are larger than that of the 1^+ multipolarity from very low incident energies. This was an additional argument to take into account contributions of all multipolarities in our calculations. It is worth mentioning that, in the μ^--capture, the 1^- multipolarity contribution dominates the total rates.

From the obtained original electron capture cross section results, we conclude that the total cross sections can be well approximated by the Gamow–Teller transitions only for low e^--energies [6,17,25,27,35]. For higher incident energies, the inclusion of contributions stemming from higher multipolarities leads to better agreement.

The above findings are in good agreement with the previous calculations performed by Cole et al. [26].

3.5. Comparison of Polar Vector and Axial Vector Contributions

In the last step of our study, we compare the separate contributions of the polar-vector operator, the axial-vector operator and their interference term originated from the corresponding components of the weak interaction Hamiltonian. Even though these contributions refer to the standard model Lagrangian, they can inspire beyond the standard model (BSM) Lagrangians in several BSM theories, as for example the one describing the muon-to-electron conversion in nuclei, where authors usually drop out the interference (polar-vector)-(axial-vector) term [51,52,60].

In Figures 5–7, we additionally illustrate the above contributions to the total electron capture cross sections. As can be seen, the main contribution to the total cross sections originates from the axial vector component and, in addition, as the incident electron energy increases, the contribution of axial vector component increases too.

This is due to the fact that the axial-vector form factors are larger than the corresponding polar-vector and the transverse terms dominate [54]. For the light nuclei, the dominance of axial-vector part is crucial, and the contribution of the other parts is negligible. As the mass number of the parent nucleus increases, the contribution of the polar-vector part grows up. For the medium-weight nuclei ^{48}Ti and ^{56}Fe, the contribution of the axial-vector is about three times larger than that of the polar-vector part. For the heavier nuclei ^{66}Zn and ^{90}Zr, the polar-vector part contributes about half of the axial-vector contribution. Finally, for all studied nuclei, the contribution of the interference term, due to the occurred cancellations, is about an order of magnitude smaller than that of the axial-vector part.

4. Summary and Conclusions

The electron capture process on nuclei plays a crucial role at the late stages of the evolution of massive stars, i.e., in pre-supernova and in core–collapse supernova phase. Thus, for understanding deeply the mechanisms governing the massive stars evolution at these phases, it is important to study extensively electron capture by calculating in detail its cross sections for hot stellar interior energies i.e., for energies at least up to 50MeV. In our present study, we assume laboratory conditions and find original (absolute) cross sections to be translated in the next step to those under stellar conditions.

By using a numerical approach based on a refinement of the pn-QRPA, describing reliably several semi-leptonic weak interaction processes, we evaluated detailed differential and total cross section of electron capture on ^{28}Si, ^{32}S, ^{48}Ti, ^{56}Fe, ^{66}Zn and ^{90}Zr isotopes (original e^--capture cross sections). Our nuclear method has been tested on the comparison of our exclusive results with the experimental and theoretical peaks of Gamow–Teller transitions. The agreement is good, providing us confidence regarding the reliability of the obtained results.

In fact, the absolute e^--capture cross sections are crucial for understanding supernova collapse and explosion. The calculated absolute cross section, however, depends on axial vector coupling constant g_A. In the present work, we used the value $g_A = 1.0$, but since the axial-vector contributions dominate, the cross section may become smaller by a factor 0.7–0.5 if we use $g_A \sim$ 0.8–0.6 (strong g_A coupling). Actually, the g_A for 1^+, 2^- derived from beta decays, muon captures and charge exchange reactions suggest much severe quenching factors than that employed here.

Our strategy in this work was to perform extensive calculations of electron capture cross sections (assuming laboratory conditions) for incident electron energies up to 50 MeV. Currently, we translate these rates to the corresponding quantities within the hot stellar environment through the use of appropriate convolution techniques assuming that leptons under stellar interior conditions follow Fermi–Dirac energy distribution. Ongoing calculations, using these cross sections, take into account the astrophysics conditions where the astrophysical e^--capture process takes place. Our method is applicable to neutrino-nucleus processes that are important in astrophysics and neutrino nucleosynthesis.

Author Contributions: Conceptualization, T.K. and H.E.; methodology, P.G. and T.K.; software, P.G.; validation, T.K. and H.E.; formal analysis, P.G.; investigation, P.G. and T.K.; resources, T.K.; data curation, P.G.; writing—original draft preparation, P.G.; writing—review and editing, T.K. and H.E.; visualization, P.G. and T.K.; supervision, T.K.; project administration, T.K.; funding acquisition, T.K. All authors have read and agreed to the published version of the manuscript.

Funding: This research received no external funding.

Institutional Review Board Statement: Not applicable.

Informed Consent Statement: Not applicable.

Data Availability Statement: Not applicable.

Acknowledgments: This research is co-financed by Greece and the European Union (European Social Fund-ESF) through the Operational Programme "Human Resources Development, Education and Lifelong Learning 2014–2020" in the context of the project (MIS 5047635). P.G. wishes to thank H. Ejiri and T. Shima for the warm hospitality at RCNP, Osaka, Japan during the NNR-19 workshop.

Conflicts of Interest: The authors declare no conflict of interest.

Appendix A. Kinematic Parameters

In Equation (4), the kinematical parameters read

$$\alpha = \frac{k_e}{E_e} = \left[1 - \left(\frac{m_e c^2}{E_e}\right)^2\right]^{1/2}, \qquad b = \frac{E_e E_{\nu_e} \alpha^2}{\mathbf{q}^2}, \qquad d = \frac{(m_e c^2)^2}{q E_e}, \tag{A1}$$

where $\mathbf{q}^2$ is the 3-momentum transfer $\mathbf{q} = \nu - k$ defined by the difference between the 3-momentum of a neutrino and of an electron.

References

1. Bethe, H.A.; Brown, G.E.; Applegate, J.; Lattimer, J.M. Equation of state in the gravitational collapse of stars. *Nucl. Phys. A* **1979**, *324*, 487. [CrossRef]
2. Bethe, H.A. Supernova mechanisms. *Rev. Mod. Phys.* **1990**, *62*, 801. [CrossRef]
3. Giannaka, P.G.; Kosmas, T.S. Electron Capture Cross Sections for Stellar Nucleosynthesis. *Adv. High Energy Phys.* **2015**, *2015*, 398796. [CrossRef]
4. Kosmas, T.S.; Tsoulos, I.; Kosmas, O.; Giannaka, P.G. Evolution of hot and dense stellar interiors: The role of the weak interaction processes. *Front. Astron. Space Sci.* **2022**, *8*, 763276. [CrossRef]
5. Giannaka, P.G. Nuclear e^--capture rates under pre-supernova nd supernova conditions. In Proceedings of the Neutrino Nuclear Responses (NNR19) for Double Beta Decays and Astro Neutrinos, Osaka, Japan, 8–9 May 2019; RCNP: Osaka University, Japan, 2019.
6. Nabi, J.U. Ground and excited states Gamow-Teller strength distributions of iron isotopes and associated capture rates for core-collapse simulations. *Astrophys. Space Sci.* **2011**, *331*, 537. [CrossRef]
7. Langanke, K.; Martínez-Pinedo, G.; Zegers, R.G.T. Electron capture in stars. *Rep. Prog. Phys.* **2021**, *84*, 066301. [CrossRef] [PubMed]
8. Martínez-Pinedo, G.; Langanke, K. Shell Model Applications in Nuclear Astrophysics. *Physics* **2022**, *4*, 677–689. [CrossRef]
9. Suzuki, T.; Honma, M.; Mao, H.; Otsuka, T.; Kajino, T. Evaluation of electron capture reaction rates in Ni isotopes in stellar environments. *Phys. Rev. C* **2011**, *83*, 044619. [CrossRef]
10. Suzuki, T.; Yoshida, T.; Kajino, T.; Otsuka, T. β decays of isotones with neutron magic number of N = 126 and r-process nucleosynthesis. *Phys. Rev. C* **2012**, *85*, 015802. [CrossRef]
11. Fuller, G.M.; Fowler, W.A.; Newman, M.J. Stellar weak interaction rates for intermediate-mass nuclei. II. A = 21 to A = 60. *Astrophys. J.* **1982**, *252*, 715. [CrossRef]
12. Aufderheide, M.B.; Fushiki, I.; Woosley, E.; Hartmann, D.H. Search for important weak interaction nuclei in presupernova evolution. *Astrophys. J. Suppl. Ser.* **1994**, *91*, 389. [CrossRef]
13. Langanke, K.; Kolbe, E.; Dean, D.J. Unblocking of the Gamow-Teller strength in stellar electron capture on neutron-rich germanium isotopes. *Phys. Rev. C* **2001**, *63*, 032801. [CrossRef]
14. Oda, T.; Hino, M.; Muto, K.; Takahara, M.; Sato, K. Rate Tables for the weak processes of sd-shell nuclei in stellar matter. *At. Data Nucl. Data Tables* **1994**, *56*, 231. [CrossRef]
15. Nabi, J.U.; Klapdor-Kleingrothaus, H.V. Weak interaction rates of $sd-$shell nuclei in stellar environments calculated in the the proton-neutron quasi-particle random-phase approximation. *At. Data Nucl. Data Tables* **1999**, *71*, 149. [CrossRef]
16. Langanke, K.; Martinez-Pinedo, G. Rate Tables for the weak processes of $pf-$shell nuclei in stellar environments. *At. Data Nucl. Data Tables* **2001**, *79*, 1. [CrossRef]
17. Nabi, J.U.; Rahman, M.U.; Sajjad, M. Electron and positron capture rates on ^{55}Co in stellar matter. *Braz. J. Phys.* **2007**, *37*, 4. [CrossRef]
18. Giannaka, P.G.; Kosmas, T.S. Electron capture on nuclei in stellar environment. *Particles* **2022**, *5*, 377–389.
19. Mori, K.; Famiano, M.A.; Kajino, T.; Suzuki, T.; Hidaka, J.; Honma, M.; Iwamoto, K.; Nomoto, K.; Otsuka, T. Impact of new Gamow–Teller strengths on explosive type Ia Supernova nucleosynthesis. *Astrophys. J.* **2016**, *833*, 179. [CrossRef]
20. Mori, K.; Famiano, M.A.; Kajino, T.; Suzuki, T.; Garnavich, P.M.; Mathews, G.J.; Diehl, R.; Leung, S.C.; Nomoto, K.I. Nucleosynthesis Constraints on the Explosion Mechanism for Type Ia Supernovae. *Astrophys. J.* **2018**, *863*, 176. [CrossRef]
21. Mori, K.; Famiano, M.A.; Kajino, T.; Kusakabe, M.; Tang, X. Impacts of the New Carbon Fusion Cross Sections on Type Ia Supernovae. *Mon. Not. R. Astron. Soc. Lett.* **2019**, 482, L70–L74. [CrossRef]
22. Brachwitz, F.; Dean, D.J.; Hix, W.R.; Iwamoto, K.; Langanke, K.; Martinez-Pinedo, G.; Nomoto, K.; Strayer, M.R.; Thielemann, F.-K.; Umeda, H. The role of electron captures in Chandrasekhar-mass models for Type Ia Supernova. *Astrophys. J.* **2000**, *536*, 934–947. [CrossRef]
23. Nabi, J.U.; Sajjad, M.; Rahman, M.U. Electron capture rates on titanium isotopes in stellar matter. *Acta Phys. Polon. B* **2007**, *38*, 3203.
24. Titus, R.; Sullivan, C.; Zegers, R.G.T.; Brown, B.A.; Gao1, B. Impact of electron-captures on nuclei near N = 50 on core-collapse supernovae. *J. Phys. G* **2018**, *45*, 014004. [CrossRef]
25. Dean, D.J.; Langanke, K.; Chatterjee, L.; Radha, P.B.; Strayer, M.R. Electron capture on iron group nuclei. *Phys. Rev. C* **1998**, *58*, 536. [CrossRef]
26. Cole, A.L.; Anderson, T.S.; Zegers, R.G.; Austin, S.M.; Brown, B.A.; Valdez, L.; Gupta, S.; Hitt, G.W.; Fawwaz, O. Gamow-Teller strengths and electron-capture rates for pf-shell nuclei of relevance for late stellar evolution. *Phys. Rev. C* **2012**, *86*, 015809. [CrossRef]
27. Zhi, Q.; Langanke, K.; Martínez-Pinedo, G.; Nowacki, F.; Sieja, K. The ^{76}Se Gamow-Teller strength distribution and its importance for stellar electron capture rates. *Nucl. Phys. A* **2011**, *859*, 172. [CrossRef]
28. Langanke, K.; Martínez-Pinedo, G. Nuclear weak-interaction processes in stars. *Rev. Mod. Phys.* **2003**, *75*, 819. [CrossRef]
29. Jing-Jing, L. Electron capture of strongly screening nuclides ^{56}Fe, ^{56}Co, ^{56}Ni, ^{56}Mn, ^{56}Cr and ^{56}V in pre-supernovae. *Mon. Not. R. Astron. Soc.* **2013**, *433*, 1108. [CrossRef]
30. Langanke, K.; Martinez-Pinedo, G. Shell-model calculations of stellar weak interaction rates: II. Weak rates for Nuclei in the mass range A = 45–65 in Supernovae environments. *Nucl. Phys. A* **2000**, *673*, 481. [CrossRef]

31. Sampaio, J.M.; Langanke, K.; Martinez-Pinedo, G.; Dean, D.J. Electron capture rates for core collapse supernovae. *Nucl. Phys. A* **2003**, *718*, 440. [CrossRef]
32. Langanke, K.; Martinez-Pinedo, G.; Sampaio, J.M.; Dean, D.J.; Hix, W.R.; Messer, O.E.; Mezzacappa, A.; Liebendörfer, M.; Janka, H.T.; Ramp, M. Electron capture rates on nuclei and implications for stellar core collapse. *Phys. Rev. Lett.* **2003**, *90*, 241102. [CrossRef]
33. Langanke, K.; Martinez-Pinedo, G. Supernova Electron Capture Rates on Odd-Odd Nuclei. *Phys. Let. B* **1999**, *453*, 187. [CrossRef]
34. Giannaka, P.G.; Kosmas, T.S. Detailed description of exclusive muon capture rates using realistic two-body forces. *Phys. Rev. C* **2015**, *92*, 014606. [CrossRef]
35. Sarriguren, P.; de Guerra, E.M.; Alvarez-Rodriguez, R. Gamow–Teller strength distributions in Fe and Ni stable isotopes. *Nucl. Phys. A* **2003**, *716*, 230. [CrossRef]
36. Sarriguren, P.; de Guerra, E.M.; Escuderos, A. β decay in odd-A and even-even proton-rich Kr isotopes. *Phys. Rev. C* **2001**, *64*, 064306. [CrossRef]
37. Kolbe, E.; Langanke, K.; Vogel, P. Comparison of continuum random phase approximation and the elementary particle model for the inclusive muon neutrino reaction on ^{12}C. *Nucl. Phys. A* **1997**, *613*, 382. [CrossRef]
38. Dzhioev, A.A.; Langanke, K.; Martínez-Pinedo, G.; Vdovin, A.I.; Stoyanov, C. Unblocking of stellar electron capture for neutron-rich N = 50 nuclei at Finite Temperature. *Phys. Rev. C* **2020**, *101*, 025805. [CrossRef]
39. Hix, W.R.; Messer, O.E.; Mezzacappa, A.; Liebendörfer, M.; Sampaio, J.; Langanke, K.; Dean, D.J.; Martínez-Pinedo, G. Consequences of nuclear electron capture in core collapse supernovae. *Phys. Rev. Lett.* **2003**, *91*, 210102. [CrossRef]
40. Zegers, R.G.T.; Department of Physics and Astronomy, Michigan State University, USA. Private communication, 2019.
41. Giraud, S.; Zegers, R.G.; Brown, B.A.; Gabler, J.M.; Lesniak, J.; Rebenstock, J.; Ney, E.M.; Engel, J.; Ravlić, A.; Paar, N. Finite-temperature electron-capture rates for neutron-rich nuclei near N = 50 and effects on core–collapse supernova simulations. *Phys. Rev. C* **2022**, *105*, 055801. [CrossRef]
42. Sullivan, C.; O'Connor, E.; Zegers, R.G.T.; Grubb, T.; Austin, S.M. The sensitivity of core-colapse supernovae to nuclear electron capture. *Astrophys. J.* **2016**, *816*, 44. [CrossRef]
43. Smponias, T.; Kosmas, O. High Energy Neutrino Emission from Astrophysical Jets in the Galaxy. *Adv. High Energy Phys.* **2015**, *2015*, 921757. [CrossRef]
44. Smponias, T.; Kosmas, O. Neutrino Emission from Magnetized Microquasar Jets. *Adv. High Energy Phys.* **2017**, *2017*, 496274. [CrossRef]
45. Kosmas, O.T.; Smponias, T. Simulations of Gamma-Ray Emission from Magnetized Microquasar Jets. *Adv. High Energy Phys.* **2018**, *2018*, 960296. [CrossRef]
46. Lau, R.; Beard, M.; Gupta, S.S.; Schatz, H.; Afanasjev, A.V.; Brown, E.F.; Deibel, A.; Gasques, L.R.; Hitt, G.W.; Hix, W.R.; et al. Nuclear Reactions in the Crusts of Accreting Neutron Stars. *Astrophys. J.* **2016**, *859*, 62. [CrossRef]
47. Juodagalvis, A.; Langanke, K.; Hix, W.; Martínez-Pinedo, G.; Sampaio, J. Improved estimate of electron capture rates on nuclei during stellar core collapse. *Nucl. Phys. A* **2010**, *848*, 454. [CrossRef]
48. Juodagalvis, A.; Langanke, K.; Martínez-Pinedo, G.; Hix, W.R.; Dean, D.J.; Sampaio, J.M. Neutral-current neutrino-nucleus cross sections for nuclei. *Nucl. Phys. A* **2005**, *747*, 87. [CrossRef]
49. Giannaka, P.G.; Kosmas, T.S. Electron-capture and its role to explosive neutrino-nucleosynthesis. *J. Phys. Conf. Ser.* **2013**, *410*, 012124. [CrossRef]
50. Chasioti, V.C.; Kosmas, T.S. A unified formalism for the basic nuclear matrix elements in semi-leptonic processes. *Nucl. Phys. A* **2009**, *829*, 234. [CrossRef]
51. Kosmas, T.S.; Faessler, A.; Simkovic, F.; Vergados, J.D. State-by-state calculations for all channels of the exotic (μ^-, e^-) conversion process. *Phys. Rev. C* **1997**, *56*, 526. [CrossRef]
52. Kosmas, T.S.; Vergados, J.D.; Civitarese, O.; Faessler, A. Study of the muon number violating (μ^-, e^-) conversion in a nucleus by using quasi-particle RPA. *Nucl. Phys. A* **1994**, *570*, 637. [CrossRef]
53. Tsakstara, V.; Kosmas, T.S. Low-energy neutral-current neutrino scattering on ^{128,130}Te isotopes. *Phys. Rev. C* **2011**, *83*, 054612. [CrossRef]
54. Balasi, K.G.; Ydrefors, E.; Kosmas, T.S. Theoretical study of neutrino scattering off the stable even Mo isotopes at low and intermediate energies. *Nucl. Phys. A* **2011**, *868*, 82. [CrossRef]
55. Balasi, K.G.; Ydrefors, E.; Kosmas, T.S. The response of ^{95,97}Mo to supernova neutrinos. *Nucl. Phys. A* **2011**, *866*, 67.
56. Tsakstara, V.; Kosmas, T.S. Analyzing astrophysical neutrino signals using realistic nuclear structure calculations and the convolution procedure. *Phys. Rev. C* **2011**, *84*, 064620. [CrossRef]
57. Ydrefors, E.; Balasi, K.G.; Kosmas, T.S.; Suhonen, J. Detailed study of the neutral-current neutrino–nucleus scattering off the stable Mo isotopes. *Nucl. Phys. A* **2012**, *896*, 1. [CrossRef]
58. Tsakstara, V.; Kosmas, T.S. Nuclear responses of ^{64,66}Zn isotopes to supernova neutrinos. *Phys. Rev. C* **2012**, *86*, 044618. [CrossRef]
59. Marketin, T.; Paar, N.; Nikšić, T.; Vretenar, D. Relativistic quasiparticle random-phase approximation calculation of total muon capture rates. *Rhys. Rev. C* **2009**, *79*, 054323. [CrossRef]
60. Kosmas, T.S.; Faessler, A.; Vergados, J.D. The new limits of the neutrinoless (μ^-, e^-) conversion branching ratio. *J. Phys. G* **1997**, *23*, 693. [CrossRef]

61. Eramzhyan, R.A.; Kuz'min, V.A.; Tetereva, T.V. Calculations of ordinary and radiative muon capture on ^{58,60,62}Ni. *Nucl. Phys. A* **1998**, *642*, 428. [CrossRef]
62. Kolbe, E.; Langanke, K.; Vogel, P. Muon capture on nuclei with $N > Z$, random phase approximation, and in-medium value of the axial-vector coupling constant. *Phys. Rev. C* **2000**, *62*, 055502. [CrossRef]
63. Kosmas, T.S. Exotic $\mu^- \rightarrow e^-$ conversion in nuclei: Energy moments of the transition strength and average energy of the outgoing e^-. *Nucl. Phys. A* **2001**, *683*, 443. [CrossRef]
64. Zinner, N.T.; Langanke, K.; Vogel, P. Muon capture on nuclei: pandom phase approximation evaluation versus data for $6 \leq Z \leq 94$ nuclei. *Rhys. Rev. C* **2006**, *74*, 024326.
65. Donnelly, T.W.; Peccei, R.D. Neutral current effects in nuclei. *Phys. Rep.* **1979**, *50*, 1. [CrossRef]
66. Zegers, R.G.T. Charge-exchange experiments with rare isotope beams for astro and neutrino physics. In Proceedings of the Neutrino Nuclear Responses (NNR19) for Double Beta Decays and Astro Neutrinos, Osaka, Japan, 8–9 May 2019; RCNP: Osaka University, Osaka, Japan, 2019.
67. Meyer, B.S. The r-, s-, and p-processes in nucleosynthesis, *Annu. Rev. Astron. Astrophys.* **1994**, *32*, 153. [CrossRef]
68. Kolbe, E.; Langanke, K.; Martinez-Pinedo, G.; Vogel, P. Neutrino-nucleus reactions and nuclear structure. *J. Phys. G* **2003**, *29*, 2569. [CrossRef]
69. Fröhlich, C.; Martinez-Pinedo, G.; Liebendörfer, M.; Thielemann, F.K.; Bravo, E.; Hix, W.R.; Langanke, K.; Zinner, N.T. Neutrino-Induced Nucleosynthesis of $A > 64$ Nuclei: The νp Process. *Phys. Rev. Lett.* **2006**, *96*, 142502. [CrossRef]
70. Toivanen, J.; Kolbe, E.; Langanke, K.; Martınez-Pinedo, G.; Vogel, P. Supernova neutrino induced reactions on iron isotopes. *Nucl. Phys. A* **2001**, *694*, 395. [CrossRef]
71. Ejiri, H.; Suhonen, J.; Zuber K. Neutrino–nuclear responses for astro-neutrinos, single beta decays and double beta decays. *Phys. Rep.* **2019**, *797*, 1. [CrossRef]
72. Ejiri, H. Nuclear Matrix Elements for β and $\beta\beta$ Decays and Quenching of the Weak Coupling g_A in QRPA. *Front. Phys.* **2019**, *7*, 30. [CrossRef]
73. Ejiri, H.; Suhonen, J. GT neutrino–nuclear responses for double beta decays and astro neutrinos *J. Phys. G: Nucl. Part. Phys.* **2015**, *42*, 055201. [CrossRef]
74. Akimune, H.; Ejiri, H.; Hattori, F.; Agodi, C.; Alanssari, M.; Cappuzzello, F.; Carbone, D.; Cavallaro, M.; Colo, G.; Diel, F.; et al. Spin-dipole nuclear matrix element for the double beta decay of ^{76}Ge by the (^{3}He, t) charge-exchange reaction. *J. Phys. G Nucl. Part. Phys.* **2020**, *47*, 05LT01. [CrossRef]
75. Langanke, K.; Martinez-Pinedo, G. Supernova electron capture rates for ^{55}Co and ^{56}Ni. *Phys. Let. B* **1998**, *436*, 19. [CrossRef]
76. Hausser, O.; Vetterli, M.C.; Fergerson, R.W.; Glashausser, C.; Jeppesen, R.G.; Smith, R.D.; Abegg, R.; Baker, F.T.; Celler, A.; Helmer, R.L.; et al. Nuclear response in the ^{54}Fe($\vec{p}, \vec{p}'$) reaction at 290 MeV. *Phys. Rev. C* **1991**, *43*, 230. [CrossRef] [PubMed]
77. Wildenthal, B.H. Empirical strengths of spin operators in nuclei. *Prog. Part. Nucl. Phys.* **1984**, *11*, 5. [CrossRef]
78. Machleidt, R. High-precision, charge-dependent Bonn nucleon-nucleon potential. *Phys. Rev. C* **2001**, *63*, 024001. [CrossRef]
79. O'Connell, J.S.; Donnelly, T.W.; Walecka, J.D. Semileptonic Weak Interactions with C^{12}. *Phys. Rev. C* **1972**, *6*, 719. [CrossRef]
80. Walecka, J.D. Semi-leptonic weak interactions in nuclei. In *Muon Physics*; Hughes, V.W., Wu, C.S., Eds.; Academic Press: New York, NY, USA, 1975; Volume 2, p. 113.
81. Ring, P.; Schuck, P. *The Nuclear Many-Body Problem*; Springer: New York, NY, USA, 1969.
82. Kaminski, W.A.; Faessler, A. Description of the ground-state pionic double charge exchange reaction on ^{128,130}Te. *Nucl. Phys. A* **1991**, *529*, 605. [CrossRef]
83. Tanaka, Y.; Oda, Y.; Petrovich, F.; Sheline, R.K. Effect of the spin-orbit potential on the single particle levels in superheavy region. *Phys. Lett. B* **1979**, *83*, 279. [CrossRef]
84. Bugaev, E.V.; Bisnovatyi-Kogan, G.S.; Rudzsky, M.A.; Seidov, Z.F. The interaction of intermediate energy neutrinos with nuclei. *Nucl. Phys. A* **1979**, *324*, 350. [CrossRef]
85. Vary, J. Private Communication. Available online: http://nuclear.physics.iastate.edu/npc.php (accessed on 1 May 2014).
86. Frekers, D. Weak interaction processes in supernovae: New probes using charge exchange reaction at intermediate energies. *Nucl. Phys. A* **2004**, *752*, 580. [CrossRef]
87. El-Kateb, S.; Jackson, K.P.; Alford, W.P.; Abegg, R.; Azuma, R.E.; Brown, B.A.; Celler, A.; Frekers, D.; Häusser, O.; Helmer, R.; Henderson, R.S. Spin-isospin strength distributions for fp shell nuclei: Results for the ^{55}Mn(n,p), ^{56}Fe(n,p), and ^{58}Ni(n,p) reactions at 198 MeV. *Phys. Rev. C* **1994**, *49*, 3128. [CrossRef] [PubMed]
88. Nabi, J.-U.; Riaz, M. Electron capture cross sections and nuclear partition functions for fp-shell nuclei. *J. Phys. G* **2019**, *46*, 085201. [CrossRef]
89. Yako, K.; Sasano, M.; Miki, K.; Sakai, H.; Dozono, M.; Frekers, D.; Greenfield, M.B.; Hatanaka, K.; Ihara, E.; Kato, M.; et al. Gamow-Teller Strength Distributions in ^{48}Sc by the ^{48}Ca(p,n) and ^{48}Ti(n,p) reactions and two-neutrino double-β decay nuclear matrix elements. *Phys. Rev. Lett.* **2009**, *103*, 012503. [CrossRef] [PubMed]
90. Rakers, S.; Bäumer, C.; Van den Berg, A.M.; Davids, B.; Frekers, D.; De Frenne, D.; Fujita, Y.; Grewe, E.W.; Haefner, P.; Harakeh, M.N.; et al. Nuclear matrix elements for the ^{48}Ca two-neutrino double-beta decay from high-resolution charge-exchange reactions. *Phys. Rev. C* **2004**, *70*, 054302. [CrossRef]
91. Jokiniemi, L.; Suhonen, J. Muon-capture strength functions in intermediate nuclei of $0\nu\beta\beta$ decays. *Phys. Rev. C* **2019**, *100*, 014619. [CrossRef]